Laterally confined growth of HMF3A induces reprogramming: Evaluating the structural changes

A thesis

submitted to

Indian Institute of Science Education and Research, Pune

In partial fulfilment of the requirements for the

BS-MS Dual Degree Programme

By

Dyuthi Sreekumar

Indian Institute of Science Education and Research, Pune

Dr. Homi Bhabha Road,

Pashan, Pune 411008, INDIA.

April 2020

Supervisor : Dr.G V Shivashankar

© Dyuthi Sreekumar 2020

Certificate

This is to certify that this dissertation entitled "Laterally confined growth of HMF3A induces reprogramming: Evaluating the structural changes" towards the partial fulfilment of the BS-MS dual degree programme at the Indian Institute of Science Education and Research, Pune represents study/work carried out by Dyuthi Sreekumar at Mechanobiology Institute, National University of Singapore under the supervision of Dr. G V Shivashankar, former Deputy Director, Mechanobiology Institute, National University of Singapore during the academic year 2019-2020.

Dr. Kundan Sengupta
Department of Biology
IISER Pune
Date: 7th March 2020

Dyuthi Sreekumar
20151059
BSMS Student
IISER Pune
Date: 7th March 2020

Declaration

I hereby declare that the matter embodied in the report entitled "Laterally confined growth of HMF3A induces reprogramming: Evaluating the structural changes" are the results of the work carried out by me at the Department of Mechanobiology Institute, National University of Singapore, under the supervision of Dr. G V Shivashankar and the same has not been submitted elsewhere for any other degree.

Dr. Kundan Sengupta
Department of Biology
IISER Pune
Date: 7ᵗʰ March 2020

Dyuthi Sreekumar
20151059
BSMS Student
IISER Pune
Date: 7ᵗʰ March 2020

Abstract

Nuclear reprogramming is a crucial event for many developmental processes and tissue repair. Although landmark studies have shown that reprogramming can be induced by external biochemical agents, the function of mechanical cue in reprogramming has not been well described. In a recent work, we showed nuclear reprogramming can be triggered by laterally confined growth of fibroblasts on fibronectin covered micropatterned with high efficiency without the introduction of any external biochemical reagents. In this study we show that human fibroblasts gain stemness properties following 8-10 days of laterally confined growth. This has been corroborated by the expression of pluripotency markers and alkaline phosphatase assays. Importantly, we describe the temporal changes of the structural components during reprogramming. Here we provide compelling evidence to show that actin cytoskeleton has a critical role in the maintenance of the geometrical features of spheroids. In addition to this, we also show the global change in H3K9Ac levels. Our finding throws light upon the unknown mechanism of mechanical cue induced somatic cell reprogramming. Taken together, this study highlights interesting facets of the spatio-temporal dynamics of structural components and epigenetic landscape during nuclear reprogramming by laterally confined growth.

Index

List of Figures and Tables:

6

Acknowledgment

Introduction

Nuclear reprogramming is a process that describes changes in the cell state that are accompanied by changes to the nuclear, epigenetic and transcriptional landscape(Apostolou and Hochedlinger, 2013). This may involve de-differentiation, a process by which a differentiated cell returns back into a state of increased pluripotency or a switch from one differentiated cell type to another (trans-differentiation) (Halley-Stott et al., 2013). In order to attain the pluripotent state, the cell must traverse through multiple roadblock and checkpoints including the cell senescence barrier, Mesenchymal to Epithelial Transition (MET), a metabolic switch acquisition of early pluripotency genes and activation of pluripotency network which is termed as reprogramming.

Early studies have reported that reprogramming somatic cells into induced pluripotent stem cells (PSCs) can be achieved in vitro through various processes like somatic cell nuclear transfer and cell fusion. Furthermore, seminal studies have shown that reprogramming can also be achieved by transduction of transcription factors as well as by chemical methods (Fig.1)(Takahashi and Yamanaka, 2015). One of the major problems with these methods is the low yield of reprogrammed cells. There have been a couple of studies that have used the mechanical cue along with biochemical factors to enhance nuclear reprogramming efficiency (Caiazzo et al., 2016; Downing et al., 2013).

In addition to chemical cues, mechanical cues have been reported to be vital to this process. Biophysical cues from cells grown on microgrooves have been shown to increase the reprogramming efficiency (Downing et al., 2013). Growing cells on 3D extracellular matrices along with biochemical factors has also been shown to increase the reprogramming efficiency compared to the conventional 2D cultures (Caiazzo et al., 2016). Culturing cells on softer matrices without the addition of any external transcriptional factors has been shown to induce reprogramming in kidney cells (Guo et al., 2014). Studies have also reported that stemness can be induced by imposed growth of cells using low adhesion surfaces into 3D spheres (Su et al., 2013).
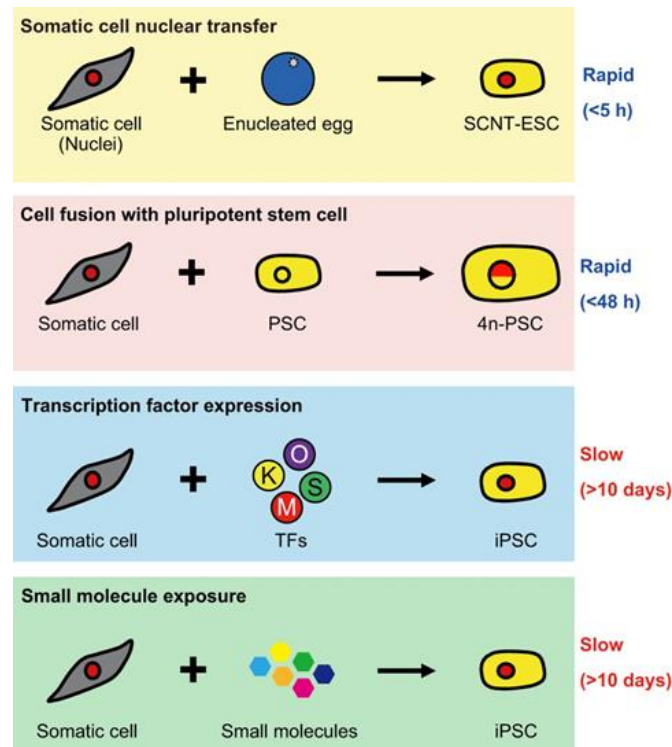
Figure 1. Methods of nuclear reprogramming. Schematic representation of various methods of reprogramming; SCNT, cell fusion, transcription factor overexpression, and through small molecule exposure. Figure taken from *Takahashi, K., and Yamanaka, S. (2015). A developmental framework for induced pluripotency. Development 142, 3274–3285.*

In vivo, cells transdifferentiate and reprogram under normal physiological stimuli (De Matteis et al., 2009). Suggesting that there might be certain microenvironmental conditions which can induce reprogramming in cells. Recent work from the lab has shown that nuclear reprogramming can be induced by prolonged laterally confined growth of NIH3T3 mouse embryonic fibroblasts on micropatterned substrates in the absence of any exogenous biochemical factors with high efficiency (Fig.2). Such laterally confined growth leads to the formation of spheroids from single cells and permitted distinct influence over the cellular geometric confinements and their mechanical properties. These reprogrammed cells exhibited erasure of epigenetic and lineage-specific marks and incorporated stemness properties (Roy et al., 2018).
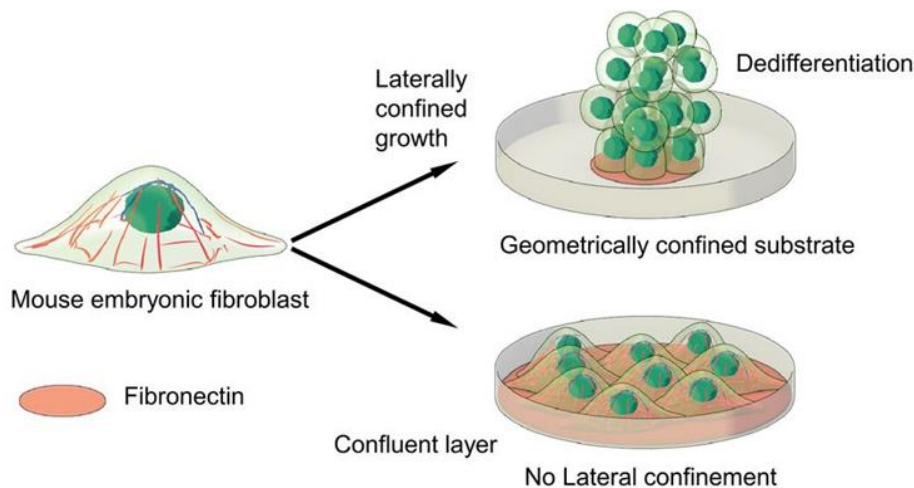
Figure 2. Laterally confined growth of cell leads to induction of pluripotent stem cell characteristics. Schematic representation of the effect of mechanical cue driven lateral confinement growth of MEFs upon dedifferention. Figure taken from *Roy, B., Venkatachalapathy, S., Ratna, P., Wang, Y., Jokhun, D.S., Nagarajan, M., and Shivashankar, G.V. (2018). Laterally confined growth of cells induces nuclear reprogramming in the absence of exogenous biochemical factors. Proc Natl Acad Sci USA 115, E4741–E4750.*

Mechanosignaling plays pivotal roles in normal physiological contexts which involves stem cell reprogramming and differentiation. Actomyosin contractility mediates a tight coupling between cytoskeletal organization, nuclear morphology, 3D chromatin organization and the transcriptome of the cell (Jain et al., 2013). Taken together, these studies underscore the importance of cell mechanics and actomyosin contractility in modulating important cellular functions. Further, studies have shown that differentiated cells and stem cells exhibit distinct nuclear and cytoskeletal organization focusing on the differences at the stage of nuclear size and chromatin compaction. For example, there are structural differences between an ES and a differentiated cell. F- actin is known to be localized near the plasma membrane in ES whereas, they appear as stress fibres in case of primary mouse embryonic fibroblasts. Chromatin structure is more open in ES cells, whereas differentiation is accompanied by a considerable increase in compaction (Fig.3). (Talwar et al., 2013). Since the cellular mechanical

state is an important regulator of cell state (Martino et al., 2018), the accompanying structural changes could be one of the key factors that drive the transition to that of a stem cell-like state. Hence, we asked if we could map these structural changes during the de-differentiation paradigm.
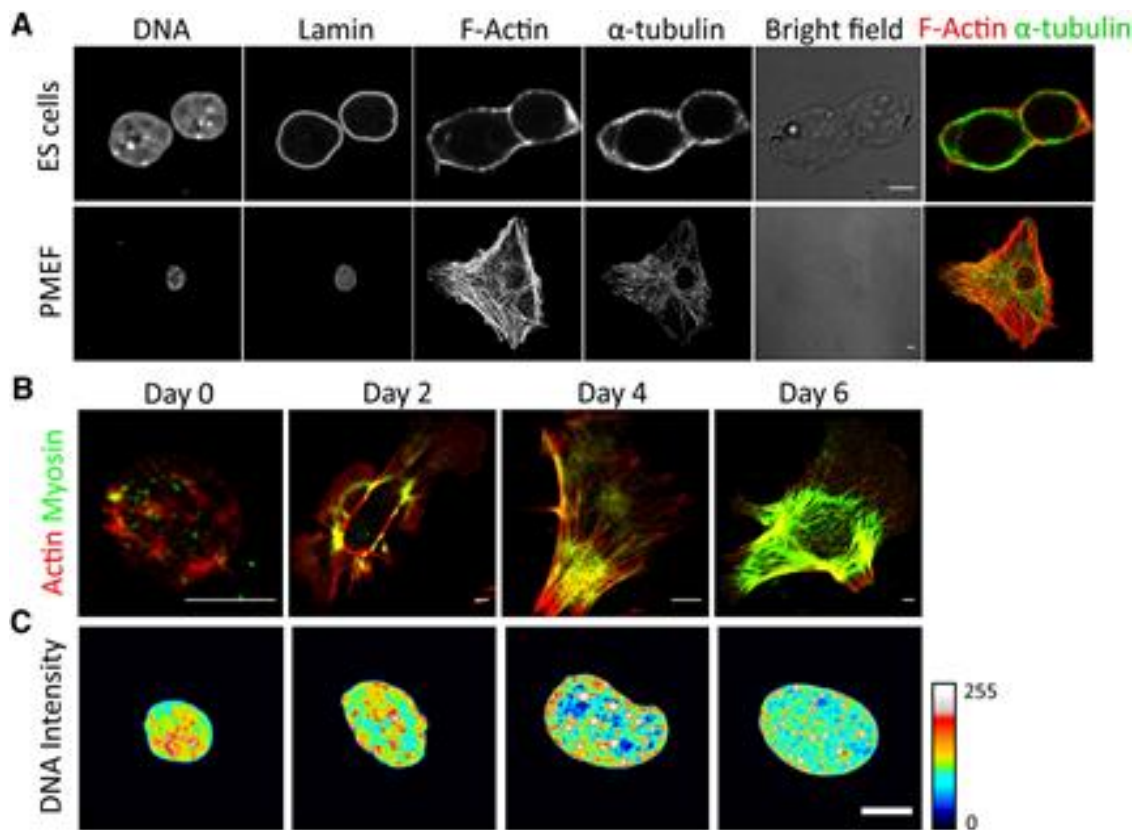
Figure 3. Cytoskeletal reorganization accompanies nuclear morphology and chromatin organization changes during differentiation. (A) Representative confocal images of ES cells and PMEF showing immunofluorescence of various structural and nuclear elements. **(B)** Representative confocal images showing actin and myosin during differentiation. **(C)** Representative confocal images showing DNA intensity; colour coding represents heterochromatin intensity. Figure taken from *Talwar, S., Kumar, A., Rao, M., Menon, G.I., and Shivashankar, G.V. (2013). Correlated spatio-temporal fluctuations in chromatin compaction states characterize stem cells. Biophys. J. 104, 553–564.*

The main goals of the study were to:

- reprogram a human fibroblast cell line in the absence of any exogenous factors
- investigate the structural changes that accompany reprogramming.

In this study we used laterally confined growth conditions to induce reprogramming in human fibroblasts. We first characterized the reprogramming potential of HMF3A cells across 8-10 days. Here we show that cells acquire stemness properties after 8-10 days of laterally confined growth conditions. Expression of pluripotency markers (Oct4, Nanog, Alkaline phosphatase) were examined from day0 to day8. We performed immunostaining to examine the dynamics of structural components (actin, pMLC, LaminA/C) during reprogramming. We also examined the physical features of the spheroids such as area, circularity and volume during reprogramming. Intervention experiments using Latrunculin A and Y27632 revealed the role of actin contractility and polymerization during the dedifferentiation process. Levels of actin, pMLC and Oct4 were quantified. The proliferation potential of these cells were characterized by Ki67 and Edu immunostaining, which showed a marked decrease with time. In addition to this, we examined the global change in the expression of H3K9Ac levels by immunostaining which showed a gradual increase temporally. Collectively, this study delineates interesting facets of the spatio-temporal dynamics of structural components and epigenetic landscape during de-differentiation.

Materials and Methods

Microcontact Printing

Fibronectin micropatterning was carried out. Polydimethylsiloxane (PDMS) elastomer (SYLGARD 184; Dow Corning) was used in a 1:10 ratio of curative-to-precursor according to the manufacturer's protocol. This mixture was poured into microfabricated silicon wafers. These wafers were degassed for 45 minutes. To prepare stamps, the wafers were kept in the oven at 80°C for 3 hours. Freshly made PDMS stamps were oxidized and sterilized under high power in Plasma Cleaner (Model PDC-002; Harrick Scientific) for 5 minutes. 10% fibronectin solution was allowed to adsorb onto the surface of each PDMS stamp under sterile condition. The PDMS stamp was then deposited onto the surface of hydrophobic dishes (ibidi) to allow transferring of the micro features. The surface was then treated with 2 mg/mL Pluronic F-127 (Sigma) for 30 min to passivate non–fibronectin-coated regions. 10,000 µm² (aspect ratio 1:5) and 3000 µm² (aspect ratio 1:5) rectangles were stamped on uncoated Ibidi dishes. These micropatterned dishes were then passivated with 0.2% pluronic acid (Sigma P2443) for 5 minutes and washed with 1x PBS.

Cell Culture and Drug Treatment

Human fibroblast cells BJ and HMF3A cells (ATCC) were grown in DMEM (Gibco; Life Technologies), supplemented with 10% (vol/vol) FBS (Gibco; Thermo Fisher Scientific) and 1% penicillin-streptomycin (Gibco; Thermo Fisher Scientific). Cells were maintained in 5% CO_2 at 37 °C. Cells between passages 20-30 were trypsinized and seeded on fibronectin-micropatterned dishes at a concentration of ~5000 cells/mL. Cells on the micropatterns were grown in previously described culture media for up to 10 days at 37 °C and 5% CO_2. The media was replaced with fresh culture media on every alternate day. Within 10 days of culture on micropatterns, the majority of cells formed tightly packed multicellular spherical bodies (spheroids). Actin filaments were depolymerized with 200 nM Latrunculin A (Sigma). Rho-associated protein kinase II (ROCK) activity was inhibited by treating cells with 20 µM Y-27632 (Sigma). HDAC activity was inhibited by treatment with 200 nM Trichostatin A (TSA). Drugs

were added from day2. Media was changed and drugs were added every alternate day.

Quantitative Real-Time PCR (qRT-PCR).

The qRT-PCR was performed to quantify the level of expression of pluripotency genes. RNA isolation was performed using RNeasy Mini kit (Qiagen) according to manufacturer's protocol. cDNA synthesis was done using iScript cDNA Synthesis kit (Bio-Rad) according to manufacturer's protocol. The qRTPCR was performed using SsoFast qPCR kit (Bio-Rad) for 40 cycles in a Bio-Rad CFX96. To quantify relative fold change in the level of genes, the qRT-PCR data were analyzed using the ΔΔCt methods with respect to GAPDH levels. The primer sequences used are listed below:

Genes	Forward	Reverse
OCT4	CGAAAGAGAAAGCGAACCAG	AACCACACTCGGACCACATC
NANOG	TGAATTTGGAAGCCACTAGGG	CCCAGATGTTGCGTAAGTCTC

Immunofluorescence Assay

Cells were fixed in 4% Paraformaldehyde (Sigma) in PBS buffer (pH 7.4) for 15 min, followed by washing with PBS (5 min × 3). Cells were permeabilized using 0.5% Triton (Sigma-Aldrich) in PBS for 15 min. After incubating with blocking solution [5% BSA (A3059; Sigma-Aldrich) in PBS] overnight at 4 °C, cells were incubated overnight at 4 °C with the primary antibodies diluted in the blocking solution. Cells were washed with PBS (10 min ×3) and incubated with corresponding fluorescent-labelled secondary antibodies diluted in blocking solution for 2 hrs at room temperature, followed by washing with PBS (10 min × 3). The nucleus was stained with NucBlue Live ReadyProbes (Molecular Probes; Thermo Fisher Scientific) in PBS for 20 min at room

temperature, and filamentous actin was stained using phalloidin Alexa Fluor 488 or 568 or 647 (1:100; Molecular Probes; Thermo Fisher Scientific) for 45 min.

Antibody information:

1.Oct4 (1:200; ab18976)

2.Nanog (1:150;CST, #4903)

3.Phospho-Myosin Light Chain 2 (1:200; CST, #3671)

4.Ki67 (1:200; CST, #9129)

5.E-Cadherin (1:200; ab76057)

6.Vimentin (1:200; CST, #5741)

7.α-Tubulin (1:200; ab15246)

8.LaminA/C (1:200; CST, #4777)

9.H3K9Ac (1:200; ab441)

Alkaline Phosphatase Staining

Cells and spheroids were fixed with 4% Paraformaldehyde (Sigma) at room temperature for 30 minutes. This was followed by washing with 1X PBS and Tris buffered saline (100 mM Tris and 5 mM MgCl2 in deionized water, pH 7.4). Further, the cells and colonies were incubated with the alkaline phosphatase substrate 5-bromo-4-chloro-3-indolyl phosphate/nitro blue tetrazolium (BCIP/NBT) (Sigma-Aldrich) at room temperature for 2 hours. This was followed by the appearance of pinkish-brown colonies over time. The dishes were observed under bright field microscopes from every half an hour to avoid oversaturation. Later, the reaction was terminated by removing the substrate solution followed by PBS wash. The number of colonies that were positive for alkaline phosphatase activity was quantified manually from the bright-field images.

Cell proliferation assay

The percentage of cells (cells grown on micropatterns) in the S phase was evaluated by using an in situ cell proliferation kit (Click-iT^{TM} EdU Alexa Fluor 555^{TM} Imaging Kit, Thermofisher scientific) that quantified the incorporation of 5-ethynyl-2'-deoxyuridine (EdU) into cellular DNA. As per the manufacturer's instructions cells were allowed to incorporate 10μM EdU for 16hrs. After EdU incorporation, cells were fixed with 4% paraformaldehyde and permeabilized with 0.5% Triton for 15 minutes. Following this, cells were incubated with 0.5mL of Click-iT® reaction cocktail for 30-35 minutes at rooM temperature and then washed with 1X PBS. Cell nuclei were counterstained with DAPI.

Image Acquisition and Analysis

Bright field images were acquired using using EVOS FL Cell Imaging System (Thermo Fisher Scientific)Confocal images were acquired using Nikon A1R laser scanning confocal microscope (Nikon Instruments Inc, Japan), using either 20x magnification (Plan Apo 20x ELWD, NA 0.8) or 40x magnification (1.25 NA water objective) with identical acquisition settings. Confocal images of 512 × 512 pixels were obtained with an XY optical resolution of 0.3μm with pinhole size 1 airy unit. In Z dimension each spheroid was scanned up to a depth of 40μm with a step size of 1μm. For calculating the reprogramming efficiency, spheroid islands were determined to be positive for Oct4 on the basis of positive (reprogrammed) and negative (non-reprogrammed human fibroblasts) thresholds.

Bright field images were quantified in ImageJ by tracing out the island boundaries for quantifying the geometrical features. The total fluorescence intensity and other geometrical features were measured for each protein in its respective channel was measured in ImageJ and IMARIS8. For image segmentation on the z-projected images, codes were written using macro in ImageJ, the following steps were performed:

1.Gaussian blurring

2.Thresholding (Huang dark)

3.Binarise

4.Convex hull

5.AND function between convex hull output and channel of interest

Statistical Analysis

All data are expressed as mean ± SD or ± SEM as noted in figure legends. For box plots the box limit represents the 25-75 percentile and whisker's 1.5x interquartile range. Each experiment was repeated at least three times. We evaluated statistical significance of the mean with the student's unpaired two-tailed t test, performed between the sample of interest and corresponding control. *p<0.05, **p<0.01. ***p<0.001.

Results

Establishing the right cell line and boundary conditions for laterally confined growth

In order to find the right boundary conditions and optimal geometric conditions for nuclear reprogramming, the cells were allowed to grow on fibronectin coated micropatterns with lateral confinement for 10 days (Fig.4A). BJ cells (Human Foreskin fibroblasts) were cultured on fibronectin-coated micropatterns with different geometries: 10,000µm² rectangle with aspect ratio 1:3 and 3000µm² rectangle with aspect ratio 1:4 (Fig.S1A,E). In both cases, the cells lost matrix attachment and rounded up instead of forming the spheroids (Fig.S1F-H). This is reflected in the area of the spheroids decreasing with time and their circularity increasing. Ultimately, we observed detachment of the cells by the end of day 10 (Fig.S1C-E). This indicates that we don't have the right boundary conditions that promote cell proliferation for BJ cells. Therefore, we switched to HMF3A (Human Mammary Fibroblasts) cells. HMF3A cells were grown on 3000µm² rectangle micropatterns (Fig.4B). Area, as well as the circularity of the HMF3A spheroids, increased with time indicating the increase in the number of cells per island as well as the formation of a spheroid (Fig.4C-E). Therefore, all future experiments were performed with HMF3A cells on 3000µm² rectangle micropatterns.

Figure 4
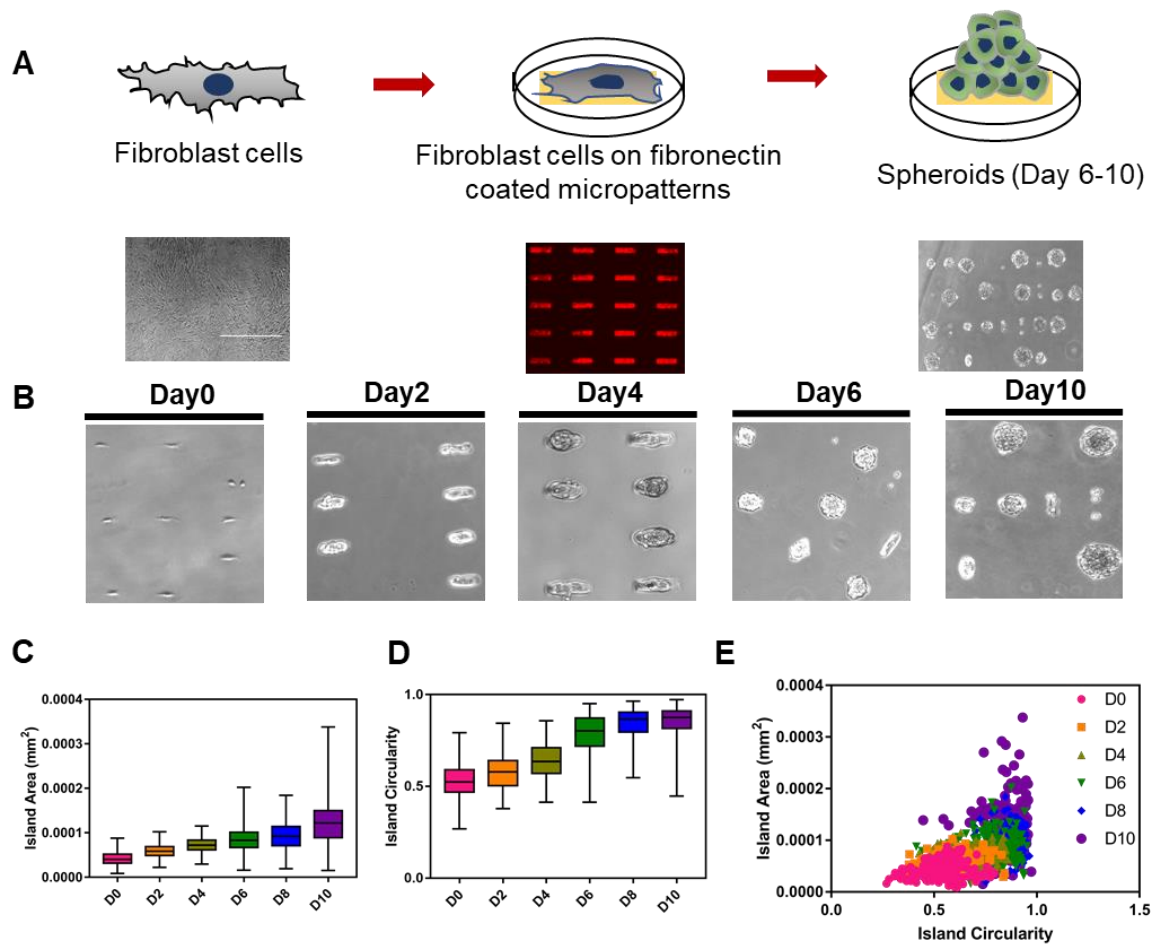
Figure 4. Selection of cell line and optimal boundary conditions. (A)
Schematic representation of laterally confined growth of fibroblasts. **(B)** Phase-contrast images of HMF3A cells cultured on 3000μm² micropatterns till day10. **(C)**
Plot represents spheroid area of BJ cells over time. **(D)** Plot represents circularity
of spheroids of BJ cells over time. **(E)** Plot represents correlation between
spheroid area and circularity of HMF3A cells on 3000μm² micropatterns. Error
bars represent SD. Scale bar = 1000μm
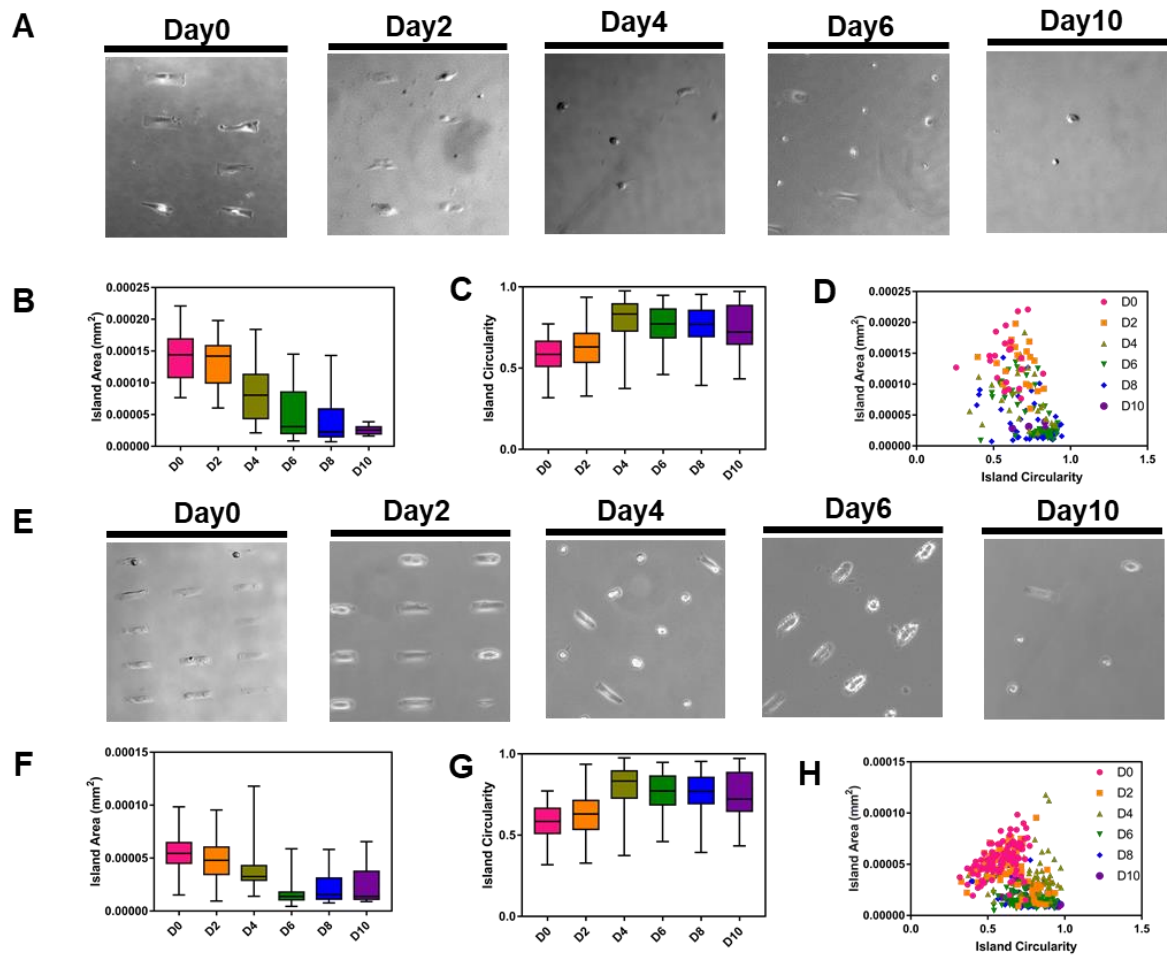
S1. Laterally confined growth of BJ cells on different micropatterns. (A) Phase-contrast images of BJ cells cultured on 10,000µm² micropatterns till day10. **(B)** Plot represents spheroid area of BJ cells over time. **(C)** Plot represents circularity of spheroids of BJ cells over time. **(D)** Plot represents correlation between spheroid area and circularity of BJ cells on 10,000µm² micropatterns. **(E)** Phase-contrast images of BJ cells cultured on 3000µm² micropatterns till day10. **(F)** Plot represents spheroid area of BJ cells over time. **(G)** Plot represents circularity of spheroids of BJ cells over time. **(H)** Plot represents correlation between spheroid area and circularity of BJ cells on 3000µm² micropatterns. Error bars represent SD.

Laterally confined growth induces stemness in HMF3A cells

We next sought to evaluate the temporal events during the reprogramming process. Since alkaline phosphatase activity is a marker for stemness property (Štefková et al., 2015), we performed this assay on day10 and day12 spheroid (Fig.5A). Remarkably, ~55% of the spheroids from day10 and 80% of the spheroids from day12 were found to be positive for alkaline phosphatase activity (Fig.5B). The control cells grown 10-12 days without lateral confinement did not show any staining for alkaline phosphatase activity (Fig.5A). We next checked the transcript levels of the bonafide reprogramming markers: Oct4 and Nanog, and found an increase in their expression (Fig.5C). Further we checked the protein expression of these marks by performing immunofluorescence (Fig.5D).

In order to evaluate the temporal progression of reprogramming events, we stained the cells with Oct4 from day 0 until day 8 (Fig.6A). The total fluorescence intensity was measured for Oct4 using the image processing pipeline outlined in Fig S2 using in-house methods. There was an increase in Oct4 levels in the spheroids with time (Fig.6E). These results confirm that lateral confinement of HMF3A cells for 8-10 days indeed induces reprogramming.

The somatic cells have to undergo various cell state transitions and checkpoints to achieve the pluripotent state. One such transition during dedifferentiation is Mesenchymal to Epithelial Transition (MET) (Li et al., 2010). Therefore, we looked at the cell state transitions during MET. We stained the cells with epithelial marker, E-cadherin and mesenchymal marker, Vimentin from day 0 to day 10 (Fig.6B,C). We observed a wave-like expression of E-cadherin with a sharp decrease at day8 (Fig.6F). In contrast, we observed a progressive decrease in the levels of Vimentin from day 2 to day 8 (Fig.6G). This implies that indeed MET is occurring during reprogramming.

Next, we went on to characterize the expression levels of structural components during reprogramming temporally. Since stem cells are known to possess softer nuclei, we intend to look at LaminA/C levels during the dedifferentiation process (Fig.6D). We observed that spheroid formation was accompanied by reduced levels of LaminA/C, indicating that the cells are becoming softer and are poised for stemness (Fig.6H).

Figure 5
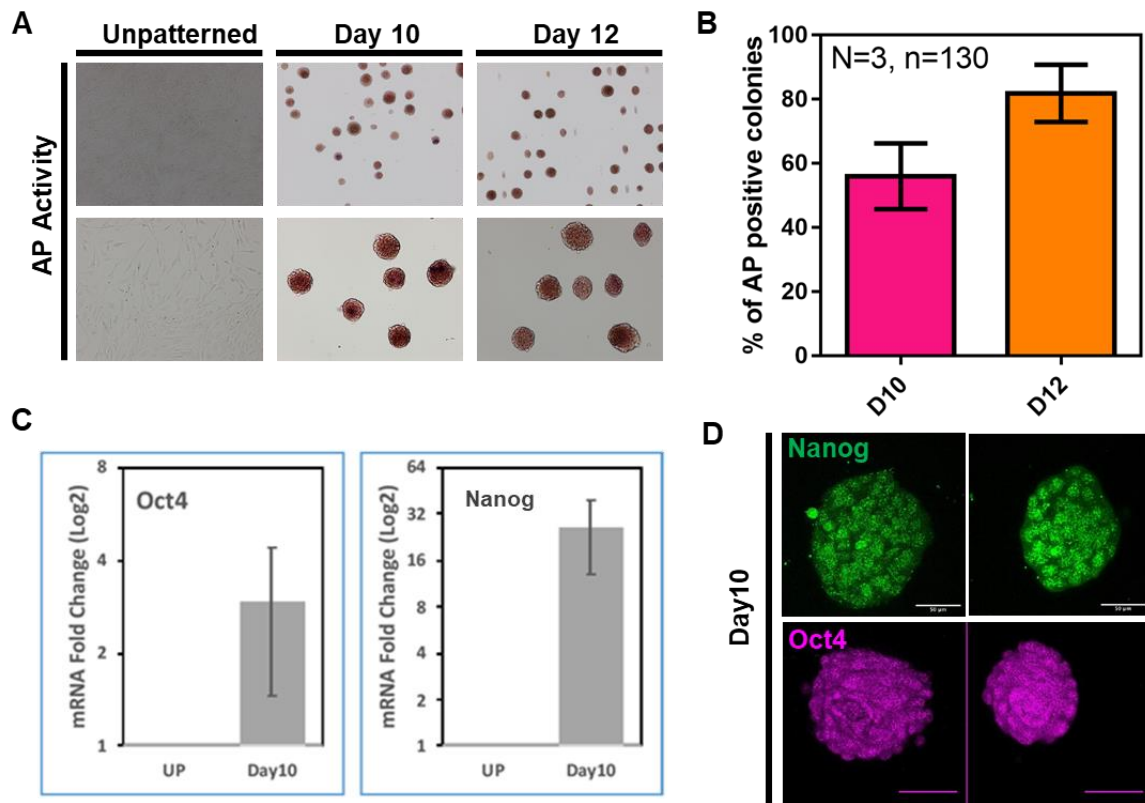
Figure 5. Laterally confined growth induces stemness in HMF3A cells. (A)
Representative bright field images showing alkaline phosphatase positive colonies in
unpatterned cells, day 10 and day 12 spheroids. **(B)** Plot showing percentage of
alkaline phosphatase positive colonies. **(C)** mRNA levels of pluripotency markers (Oct4
and Nanog) at day 10. **(D)** Representative confocal z-stack images showing Oct4 and
Nanog positive spheroids at day 10.

Figure 6
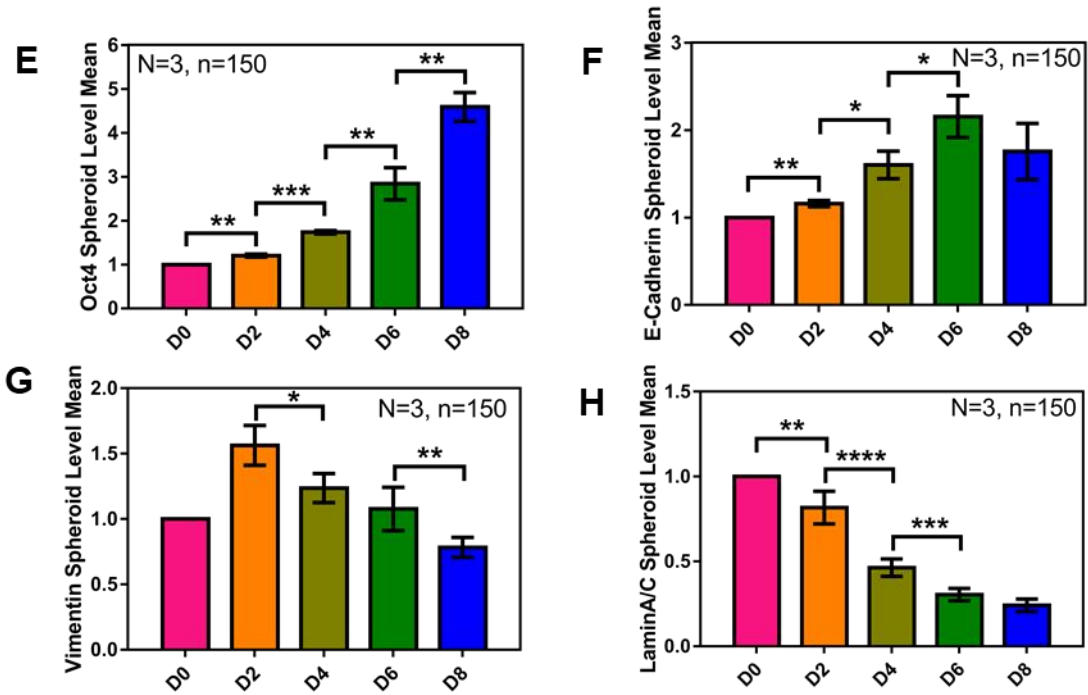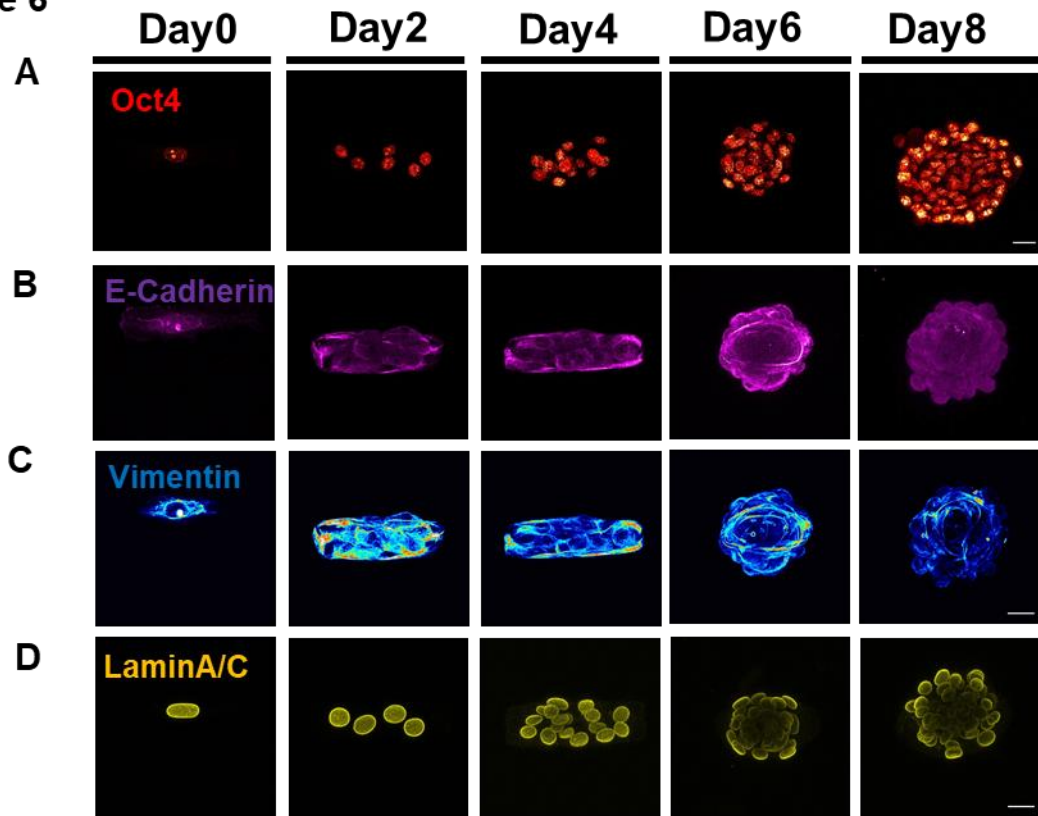
Figure 6. Temporal evaluation of cell states and structural components during reprogramming. Representative confocal z-stack images showing **(A)** Oct4, **(B)** E-Cadherin, **(C)** Vimentin and **(D)** LaminA/C staining at day0,2,4,6 & 8 respectively. **(E-F)** Plot showing Oct4, E-Cadherin, Vimentin and LaminA/C intensity of spheroids with time. (All the above mentioned data were plotted from 3 independent biological replicates. Error bars represent mean±SEM, Significance was calculated using t-test *p<0.05, **p<0.01. ***p<0.001). Scale bar = 20μm

S2

z-projected image
(cytoskeletal channel)

Gaussian blurring

Binarize

AND
Function

Channel 'n'

Convex hull

Compute features (Area, Circularity,
Total Intensity etc..)
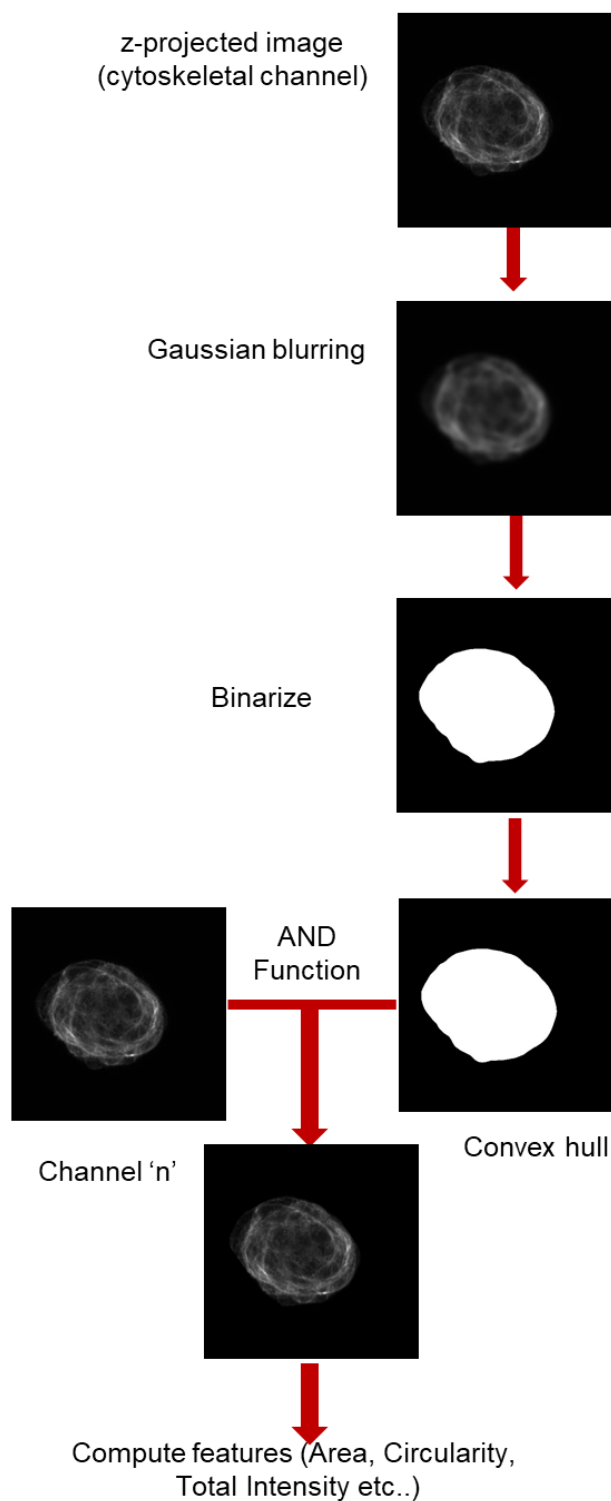
S2. Schematic representation of image processing strategy.

Repeated cell divisions are required for reprogramming

We qualitatively observed an increase in height of the spheroid (Fig.7A,Y-Z axis). We also observed an increase in area and circularity of spheroids with time (Fig.S3A,B). Cell proliferation rate is also known to control the efficiency of somatic cell reprogramming (Ruiz et al., 2011). Therefore, we sought to inquire whether repeated cell divisions are required to gain stemness during laterally confined growth. For this we used EdU (5-ethynyl-2'-deoxyuridine), which is a thymidine analogue to stain the cells that had proliferated during the last 24hrs. This will identify the number of cells that had entered the S phase within the past 24 hrs. The cells were incubated with the cocktail mix (detailed protocol given in Materials and Methods) prior to the day of fixation. The fixed cells were stained with EdU from day2 to day8 (Fig.7B). We observed a significant decrease in EdU levels over time. Furthermore, the cells were also stained with Ki67, which is a known cellular marker for cell proliferation (Scholzen and Gerdes, 2000) (Fig.S3C). Consistent with the EdU results, we observed a significant decrease in proliferation rate with time (Fig.S3D). Interestingly, we observed that the smaller spheroids day 8 did not show any staining for EdU. Therefore, we wanted to know if proliferation rate is dependent upon the size of the spheroid. Hence, we plotted the correlation between total intensity and spheroid area for day 8 spheroids. We indeed observed a positive correlation between spheroid area and EdU intensity. This shows that smaller spheroids at day 8 have stopped proliferating.

Since we observe spheroids of different sizes at Day 10 (Fig.7E) we asked if these physical features correlate with reprogramming efficiency as measured by Oct4 levels. We find that the spheroid size and circularity are correlated with reprogramming efficiency at day 10 and at all time points (Fig.7F,G & S3E,F). This suggests that multiple cell divisions and the formation of a spheroid are required for reprogramming. Therefore, variable growth kinetics could contribute to the heterogeneity observed in the reprogramming efficiencies.

Figure 7

A

Day0   Day2   Day4   Day6   Day8

DAPI
Actin

B

Day2   Day4   Day6   Day8

DAPI
EdU

C

N=3, n=90

EdU Spheroid Level Mean

D2   D4   D6   D8

D

Pearson r=0.704

Spheroid Area (μm²)

EdU Spheroid level Mean (a.u.)

E

DAPI
Actin

Oct4

F

Pearson r=0.87

Spheroid Area (μm²)

Oct4 Spheroid level Mean at Day 10 (a.u)

G

Pearson r=0.87

Circularity (a.u)

Oct4 Spheroid level Mean at Day 10 (a.u)

27
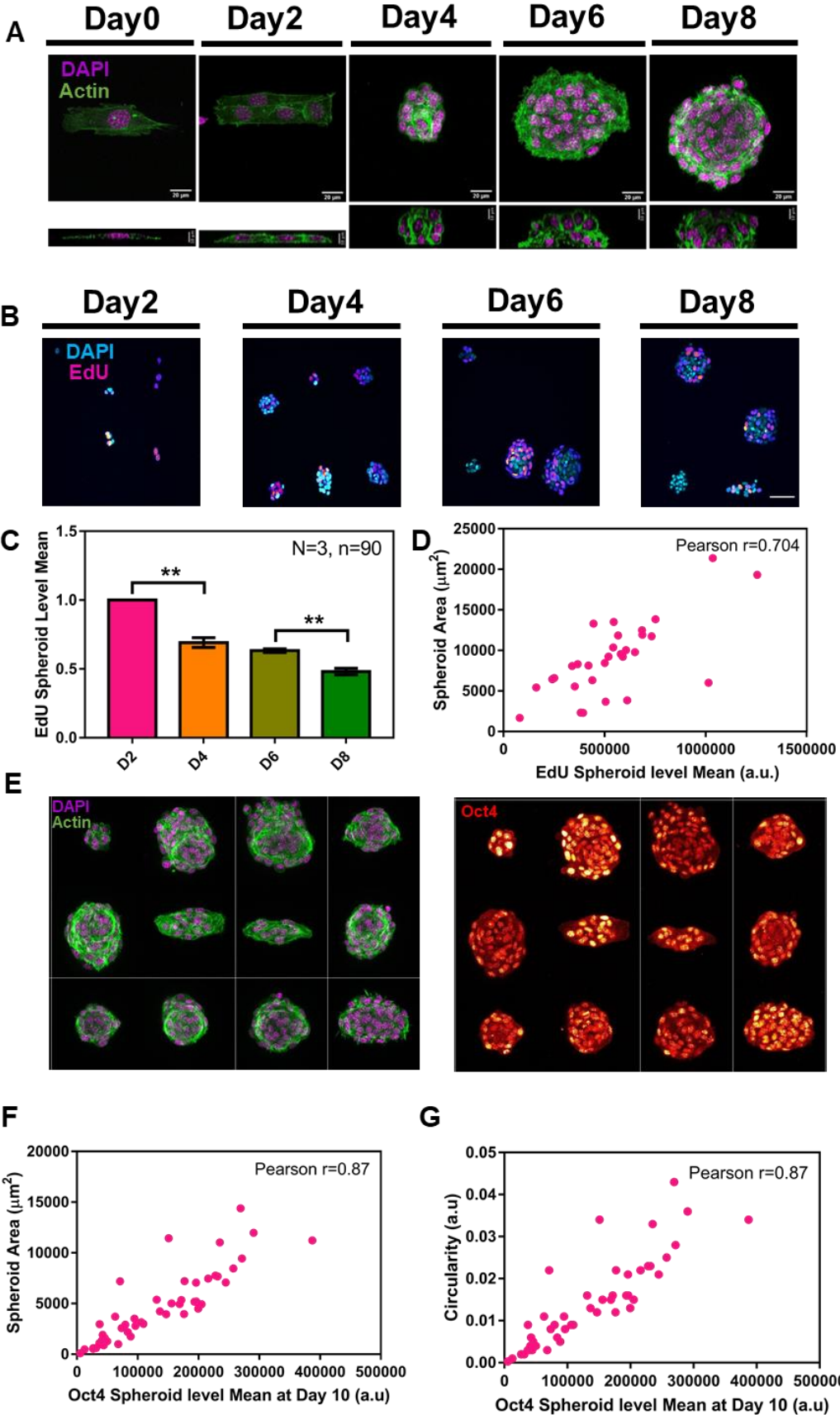
Figure 7. Repeated cell divisions are required for gaining stemness (A) Representative confocal z-stack images showing DAPI and F-actin staining at day0,2,4,6 & 8 respectively. **(B)** Representative confocal z-stack images showing DAPI and EdU staining at day2,4,6 & 8 respectively. **(C)** Plot showing EdU intensity of spheroids with time. **(D)** Box plots showing Oct4 intensity of spheroids with time. **(E)** Montage showing confocal z-stack of DAPI, F-actin and Oct4 staining at day 10. **(F,G)** Scatterplot showing correlation between Total Oct4 Intensity of day 10 spheroids versus Area and Circularity respectively. Scale bar = 20μm.
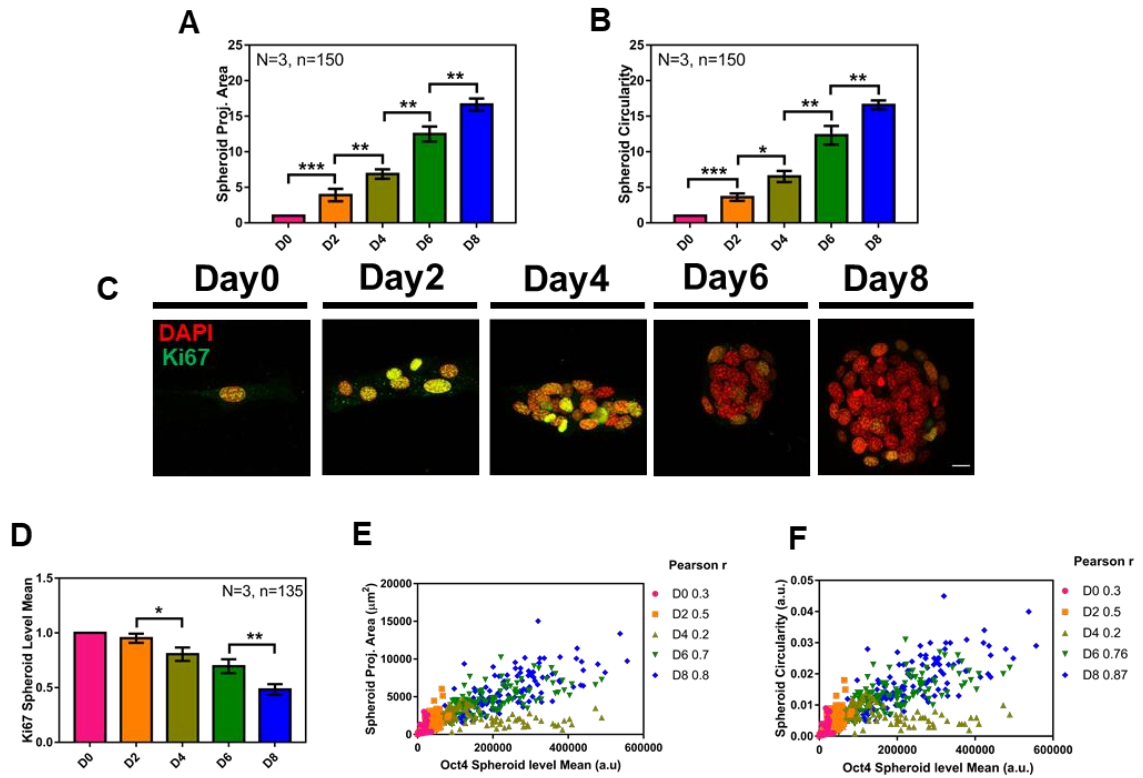
S3. Repeated cell divisions are required for gaining stemness (A) Plots showing spheroid area with time. **(B) P**lots showing spheroid circularity with time. **(C)** Representative confocal z-stack images showing DAPI and Ki67 staining at day2,4,6 & 8 respectively. **(C)** Plot showing Ki67 intensity of spheroids with time. **(D)** Box plots showing Oct4 intensity of spheroids with time. **(E,F)** Scatterplot showing correlation between Total Oct4 Intensity of spheroids versus Area and Circularity respectively. Scale bar = 20μm.

Actin contractile rings maintain the shape of the spheroid and are important for gaining stemness

Stem cells have very little cytoskeleton and are less contractile (Ambriz et al., 2018). We were therefore interested in whether the F-actin levels and contractility changes with spheroid formation and whether a decrease in actin contractility correlated with the reprogramming efficiency. Hence we stained the cells with filamentous actin (F-actin) and pMLC (Phosphorylated Myosin Light Chain), which is a marker for active myosin II motors and cytoskeletal contractility (Fig.8A) (Kasza et al., 2009). We observed an increase in F-actin levels (Fig.8B) and a decrease in actin contractility over time (Fig.8C). Interestingly, we observed F-actin ring formations from day4 (Fig.8A). We next asked what is the role of these filaments in reprogramming.

We hypothesized that the formation of these actin rings is important to the maintenance of spheroid structure and thereby involved in the reprogramming process. We went on to see the effect of actin polymerization on reprogramming efficiency. Latrunculin A, which is an actin depolymerizing drug (Ihnatovych et al., 2009) was added to the cells from day 0 and day 6 respectively (Fig.8D). Media was changed and the drug was added every alternate day. The cells were cultured till day10 and were stained for F-actin and Oct4 (Fig.8E). We observed a significant reduction F-actin upon treatment with latrunculin A (Fig.S4B). We observed a significant reduction in the levels of Oct4 (Fig.8F). There was also a significant decrease in area of the spheroid as well as a decrease in circularity upon addition of latrunculin A (Fig.8G,S4C). This suggests there is less cell proliferation and actin structure is involved in the shape of the spheroid.

We therefore tested the effect of depletion of actin contractility on the reprogramming efficiency. Y27632, which is an inhibitor of rock associated protein kinase II (ROCKII), which is a regulator of actomyosin contractility (Liao et al., 2007) was added to the HMF3A cells grown on micropatterns (20µM) from day 2 and day 6 respectively. The cells were cultured till day 10, fixed and stained for pMLC and Oct4 (Fig.8H). There was a significant reduction in pMLC levels upon addition of Y27632 from day 0 (Fig.S4D). Interestingly, we observed a significant reduction in the levels of Oct4 upon addition of Y27632 (Fig.8D). We also observed a significant increase in area and a

decrease in circularity upon treatment with Y27632 (Fig. S4E,8J). This suggests there is more cell proliferation with Rock inhibition, which is in agreement with other studies (Wang et al., 2017). Further, the increase in aspect ratio shows that actin contractility is involved in maintaining the shape of the spheroid.

These results suggest that the actin ring observed is a contractile structure that is a pivotal element in the maintenance of the sphericity of these spheroids.
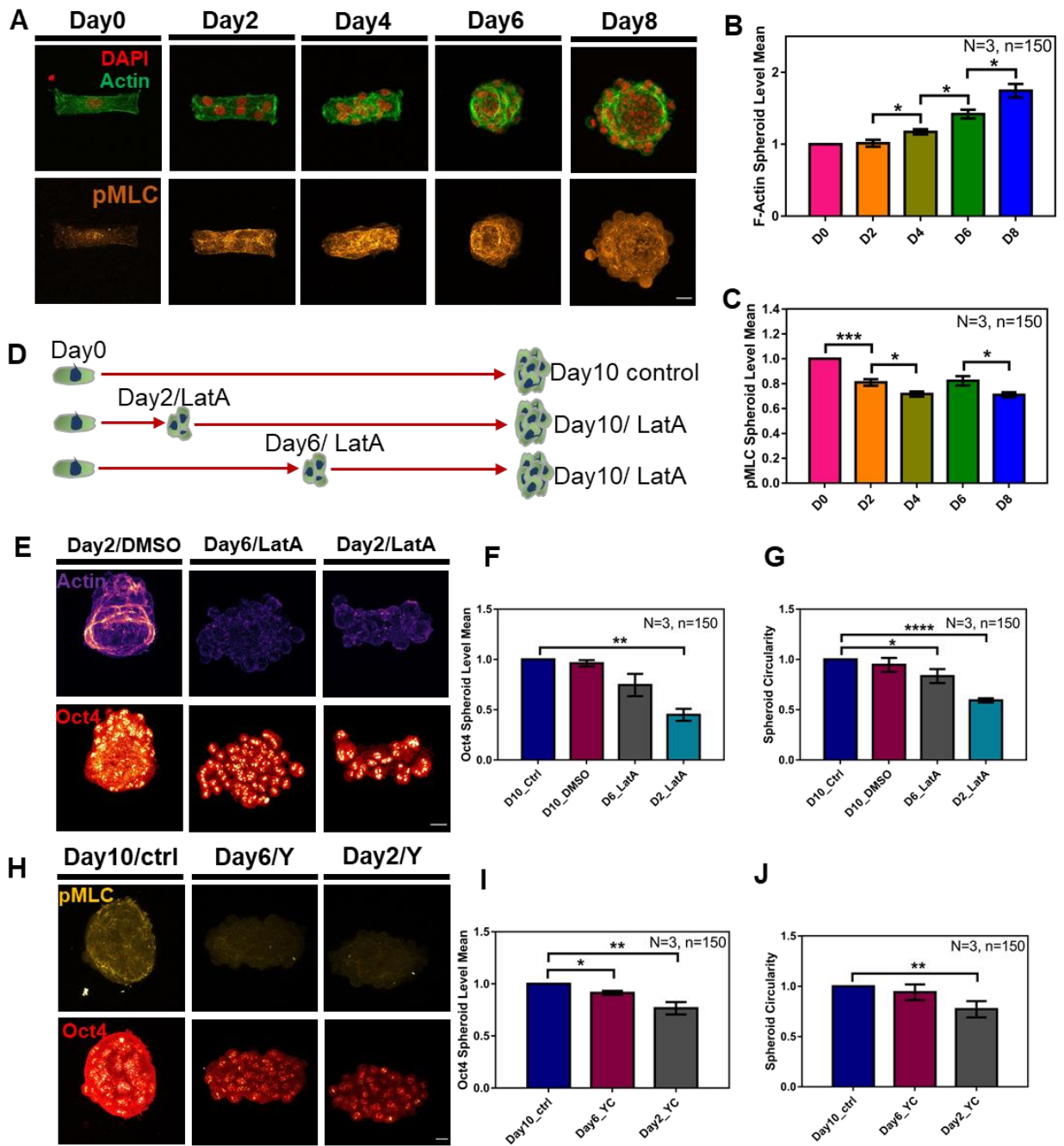
Figure 8

Figure 8. Role of actin contractile rings in reprogramming. (A) Representative confocal z-stack images showing F-actin and pMLC staining at day0,2,4,6 & 8 respectively. **(B,C)** Plot showing F-actin and pMLC intensity of spheroids with time. **(D)** Schematic of experimental setup. **(E)** Representative confocal z-stack images showing F-actin and Oct4 staining for day10 control, day6/LatA and day2/LatA respectively. **(F)** Plot showing Oct4 intensity of spheroids. **(G)** Plot showing spheroid circularity. **(H)** Representative confocal z-stack images showing pMLC and Oct4 staining for day10 control, day6/Y and day2/Y respectively. **(I)** Plot showing Oct4 intensity of spheroids. **(F)** Plot showing spheroid circularity. (All the above mentioned data were plotted from 3 independent biological replicates. Error bars represent mean±SEM, Significance was calculated using t-test *p<0.05, **p<0.01. ***p<0.001). Scale bar = 20µm

S4
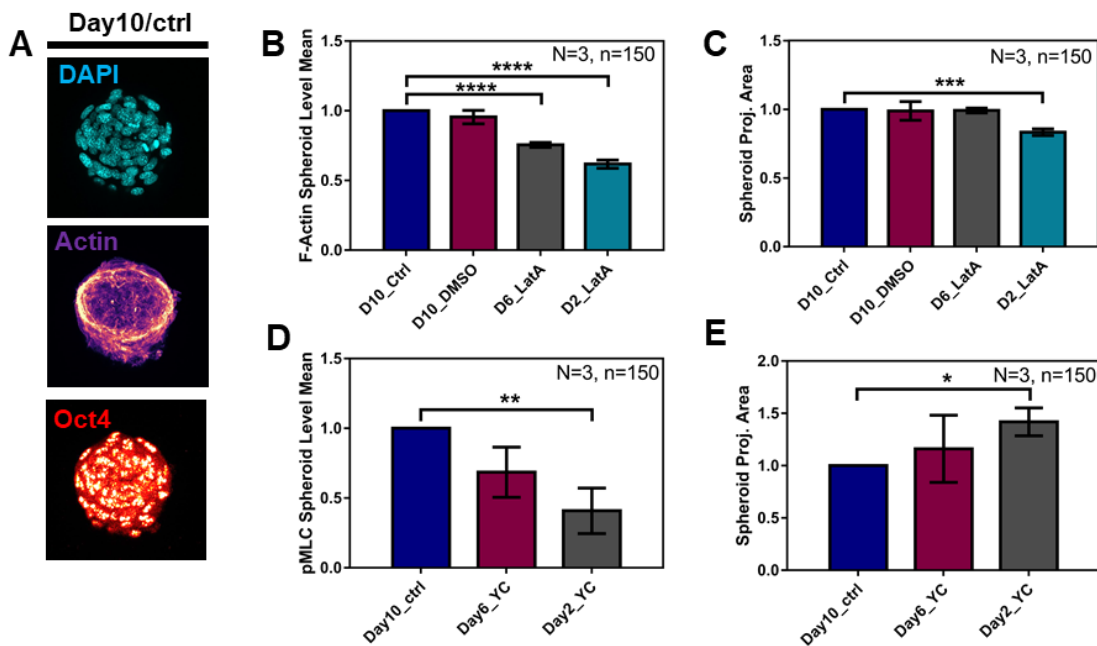
S4. Actin rings are important in maintaining spheroid shape. (A) Representative confocal z-stack images showing DAPI, F-actin and Oct4 staining for day10 control **(B)** Plot showing F-actin intensity of spheroids. **(C)** Plot showing spheroid area. **(D)** Plot showing pMLC intensity of spheroids. **(E)** Plot showing spheroid area.

Chromatin compaction is linked to reprogramming efficiency

Recent evidence from imaging of chromatin structures indicate that undifferentiated ES and iPSCs exhibit an open chromatin state compared to the differentiated cells (Gaspar-Maia et al., 2011). H3K9Ac is known to be a part of the active promoter state (Karmodiya et al., 2012). Hence, we intend to check the global levels of H3K9Ac, levels during reprogramming. We stained the cells with H3K9Ac from day 0 to day 8 (Fig.9A). We observed a gradual increase in H3K9Ac levels with time (Fig.9B).

The genome of pluripotent cells are characterized by decondensed chromatin and distinct epigenetic features (Gaspar-Maia et al., 2011). Therefore, we went on to see the effect of chromatin compaction on reprogramming efficiency. Trichostatin A (TSA), which is a specific inhibitor of histone deacetylase (HDAC) activity (Vigushin et al., 2001) was added to the cells from day 0 and day 6 respectively (Fig.9C). TSA interferes with the ability of the transcription factors to access the DNA inside the chromatin (Drummond et al., 2005). Media was changed and the drug was added every alternate day. The cells were cultured till day10 and were stained for Oct4 (Fig.9D). We observed a significant increase in Oct4 levels upon treatment with TSA (Fig.9E). However, we did not observe any significant change with the geometrical features of the spheroid such as area, aspect ratio and roundness upon TSA treatment (Fig.S5A-C). Hence, decreasing the compaction of the chromatin results in more efficient reprogramming.

Figure 9. Chromatin compaction is linked to reprogramming efficiency. (A) Representative confocal z-stack images showing H3K9Ac staining at day0,2,4,6 & 8 respectively. **(B)** Plot showing H3K9Ac intensity of spheroids with time. **(C)** Schematic of experimental setup. **(D)** Representative confocal z-stack images showing Oct4 staining for day10 control, day6/TSA and day2/TSA respectively. **(E)** Plot showing Oct4 intensity of spheroids. (All the above mentioned data were plotted from 3 independent biological replicates. Error bars represent mean±SEM, Significance was calculated using t-test *p<0.05, **p<0.01. ***p<0.001). Scale bar = 20µm
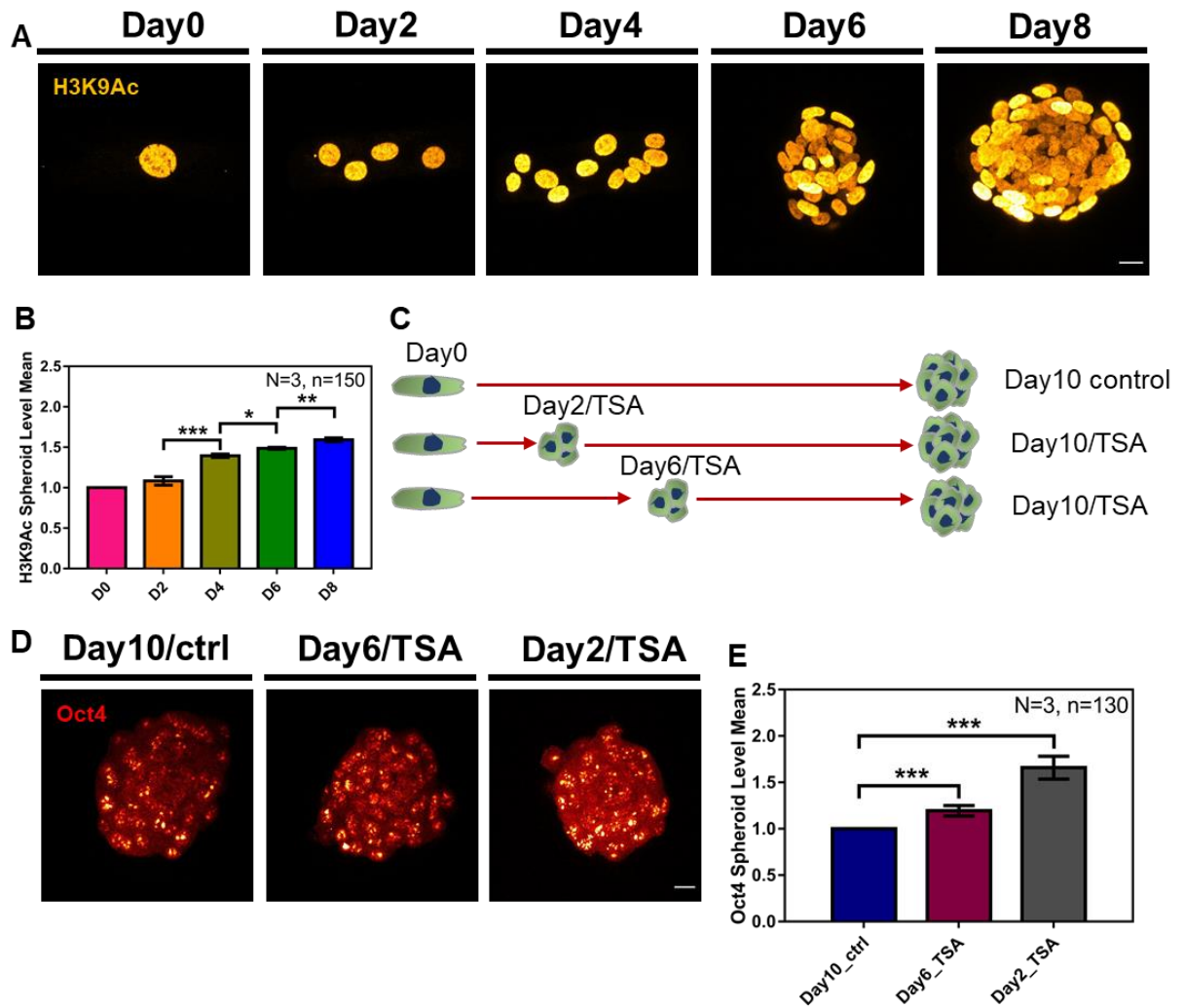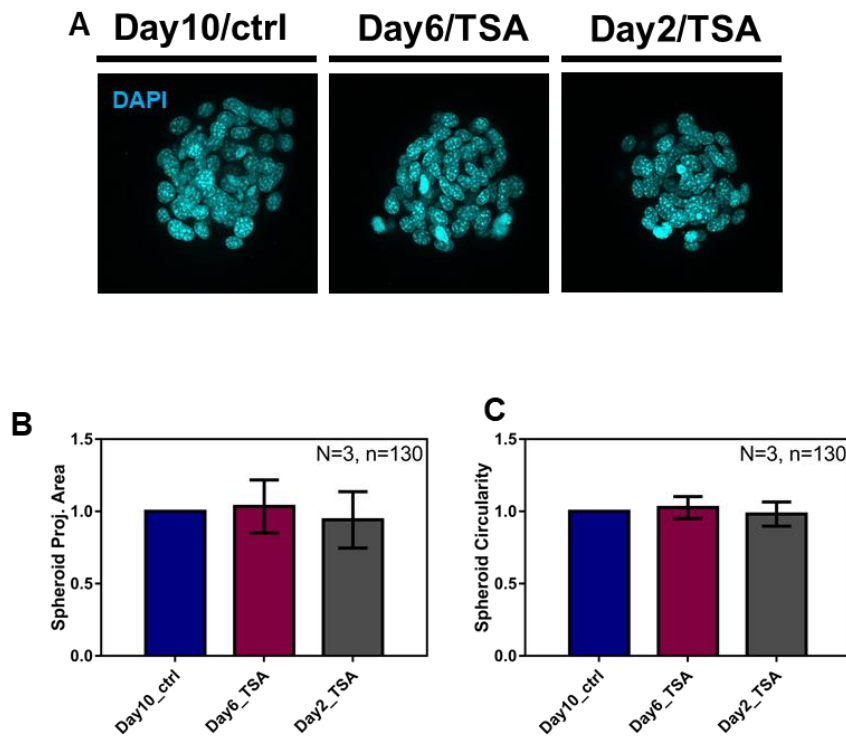
S5

S5. Chromatin compaction is linked to reprogramming efficiency. (A) Representative confocal z-stack images showing DAPI staining for day10 control, day6/TSA and day2/TSA respectively. **(B)** Plot showing spheroid area. **(B)** Plot showing spheroid circularity.

Discussion

iPSCs, somatic cell nuclear transfer and small molecules have been used in nuclear reprogramming processes in various studies such as reprogramming of T cells, cardiac cells and skin tissue (Takahashi and Yamanaka, 2006) (Gurdon, 1962). Landmark experiments have shown that nuclear reprogramming can be induced by the overexpression of certain transcription factors such as OSKM factors as well (Gurdon and Melton, 2008) (Takahashi and Yamanaka, 2016). Although these techniques have immense applications, due to their low efficiency and high risk of genetic mutations due to oncogenic transformations acquired during the reprogramming process, their clinical use is limited.

In our previous study, we've shown that nuclear reprogramming can be induced by allowing cells to grow on lateral confined growth conditions for 10 days (Roy et al., 2018). Here, in this study we've shown that prolonged growth of human fibroblasts on these micropatterns promote stemness with high reprogramming efficiency (~50-80%) when compared to other methods. Transcript level increase in stem cell transcription factors such as Oct4 and Nanog as well as positive colonies for alkaline phosphatase activity provide concomitant evidence that reinforce the pluripotency in day 10 spheroids. Temporal evaluation of reprogramming events by immunofluorescence also revealed compelling evidence that supports the idea the stemness properties increase over time.

Cellular proliferation is an essential event during the dedifferentiation process (Xu et al., 2013). Studies have suggested that a high proliferation rate is required for high reprogramming efficiency which crosses the senescent barrier and by reduced apoptosis rates (Son et al., 2013) (Ruiz et al., 2011). Interestingly, in our model of mechanical cue induced reprogramming we have shown that the dedifferentiation process is progressed by reduced proliferation rates over time. Spheroid level analysis of bonafide proliferation marker Ki67 and EdU cell proliferation assay suggested that there is a progressive reduction in the proliferation rate with time. Importantly, we see that some spheroids stop proliferations at various time points. This leads to the

variability in the shapes and sizes of spheroids at Day10. Further, we find that only large and circular spheroids exhibit reprogramming markers. These results suggest that the growth kinetics of the spheroid are linked to its reprogramming efficiency.

Reprogramming is accompanied by many cell state transitions. Cells on our reprogramming platform indeed overcomes the MET barrier in order to undergo reprogramming. Mesenchymal cells transition to Epithelial cells which are further transformed to reprogramming cells in our system. Cell state transitions are also accompanied and aided by distinct cytoskeletal and nuclear architecture changes during the de-differentiation paradigm (Uhler and Shivashankar, 2016). Reduced levels of LaminA/C over time indicates that the nuclei of the spheroids are becoming softer and they are indeed poised towards stemness.

We also observed that there was a decrease in overall contractility but we saw an increase in F-Actin levels, particularly in the shape of a ring from Day 4 of culture. This is unlike other reprogramming models, where iPSCs are known to have little cytoskeleton, our model showed an increase in F-actin levels over time. Intervention experiments with latrunculin and Y27632 revealed that the reprogramming efficiency is in fact reduced when then the rings are depleted. Apart from reduced Oct4 levels, the circularity of the spheroid such as area was significantly decreased. This suggests that the F-actin ring plays an important role in maintaining the shape of the spheroid. Based on these results, we infer that the maintenance of the shape is crucial during the reprogramming process.

Nuclear reprogramming involves a change in epigenetic landscape, i.e, it involves erasure of various epigenetic marks and rewiring of the genome organization (Halley-Stott and Gurdon, 2013). We report an increase in H3K9Ac levels over time during laterally confined growth. This impinges the fact that the fibroblasts that are reprogrammed under laterally confined growth conditions undergo chromatin decondensation. Intervention experiments with TSA revealed that reprogramming efficiency is indeed increased during the open chromatin state. Apart from this model's

high efficiency of reprogramming, we have shown that the efficiency can be further increased upon addition of small molecules.

Apart from these interesting results, there are a few limitations to our model system. The initial conditions may not be 100% homogenous, i.e., there could be doublets or triplets at day 0. However, it was made sure that ~80-90% of the islands contain only singlets at day 0. Furthermore, it was not possible to check the transcript levels of our candidate genes temporally since the initial sample size of day 0 is very low (5000 cells/mL). We presume that our study has major implications in the physiological settings, as there remains a finite possibility for cells to reprogram within our tissues. Our model system could help us in understanding the biophysical factors that are involved in cell fate regulation in diseased conditions.

In summary, we demonstrated that the laterally confined growth of human fibroblasts on fibronectin coated micropatterns induces reprogramming and confers on them ES-like characteristics with high efficiency. We also highlight the role of cytoskeletal forces and chromatin structure in controlling the efficiency of this process (Fig.10). Our study underscores an unexplored function of mechanical cues in nuclear reprogramming. An important association of our model in the local physiological context is for example due to a wound like condition the neighbouring fibroblasts could potentially experience reprogramming in the confined intervening gaps. Our observation presents a distinct method to improve existing stem cell technologies for deriving patient specific disease models, suggesting its potential application in tissue engineering and regenerative medicine.
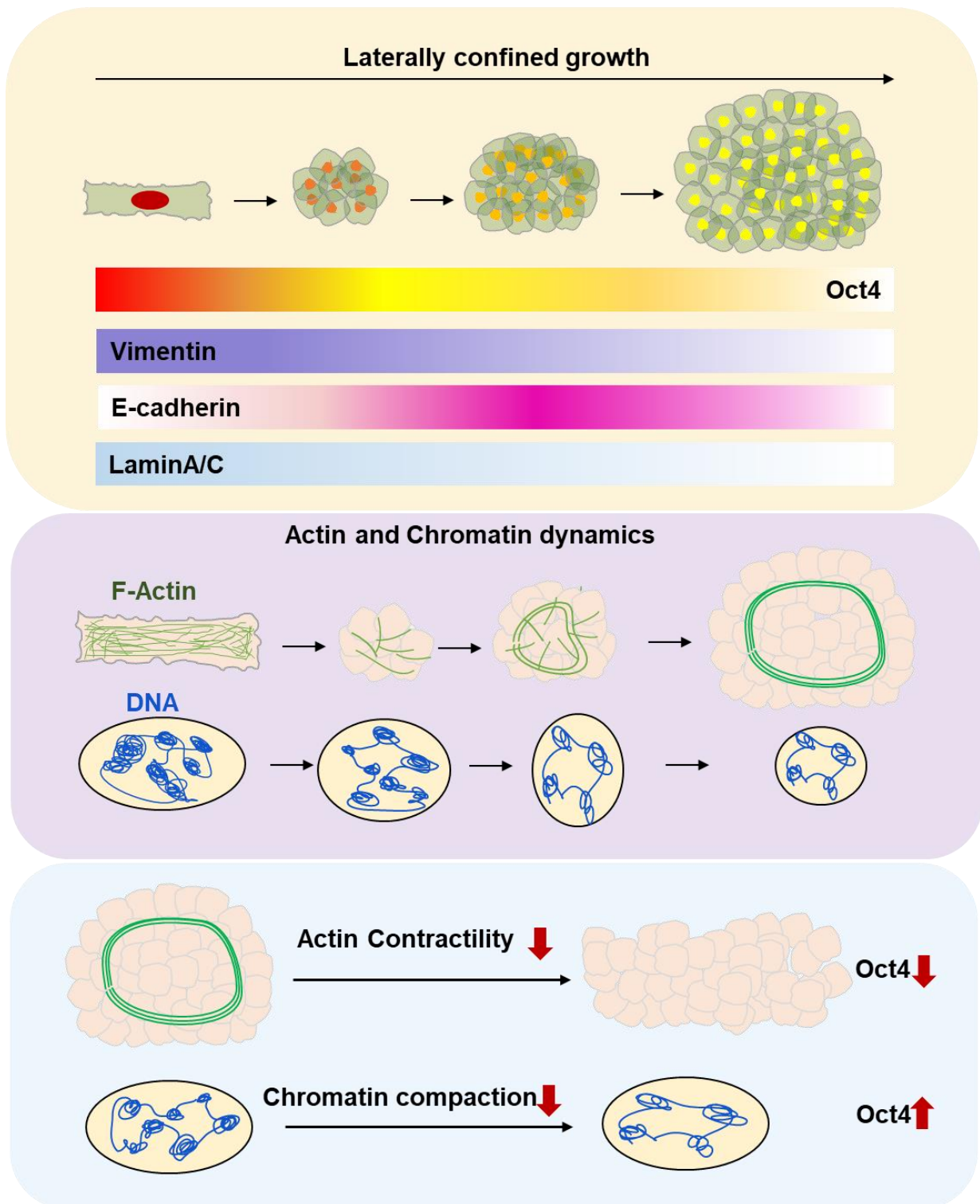
Figure 10

Figure 10. Summary. Schematic of reprogramming by laterally confined growth of human fibroblasts and accompanying structural changes.

Future directions

In this study, we have shown that an increase in size of spheroid and the accompanying structural changes are indicative of an advanced stage in reprogramming. Therefore, the transcriptome of spheroids of different sizes would describe the transient stages of cells during reprogramming (Fig.11). In order to identify the different stages in reprogramming, RNA-seq of single spheroids can be performed in day10 spheroids. This will enable us to identify candidate genes that are deregulated in various stages of the spheroid. This will in turn guide us in capturing the transcriptional heterogeneity from different spheroids of varying sizes and shapes. Furthermore, these stages can also be captured by analyzing the heterogeneity in spheroid morphologies, intensity and chromatin features.
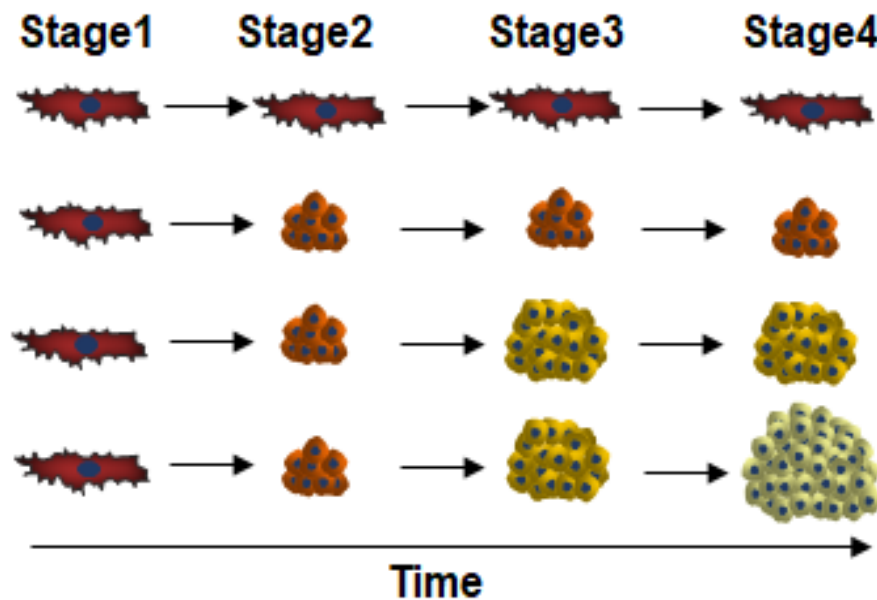

Figure 11. Schematic representing speculative intermediary stages during reprogramming

References:

1. Ambriz, X., de Lanerolle, P., and Ambrosio, J.R. (2018). The Mechanobiology of the Actin Cytoskeleton in Stem Cells during Differentiation and Interaction with Biomaterials. Stem Cells Int. *2018*, 2891957.

2. Apostolou, E., and Hochedlinger, K. (2013). Chromatin dynamics during cellular reprogramming. Nature *502*, 462–471.

3. Caiazzo, M., Okawa, Y., Ranga, A., Piersigilli, A., Tabata, Y., and Lutolf, M.P. (2016). Defined three-dimensional microenvironments boost induction of pluripotency. Nat. Mater. *15*, 344–352.

4. De Matteis, R., Zingaretti, M.C., Murano, I., Vitali, A., Frontini, A., Giannulis, I., Barbatelli, G., Marcucci, F., Bordicchia, M., Sarzani, R., et al. (2009). In vivo physiological transdifferentiation of adult adipose cells. Stem Cells *27*, 2761–2768.

5. Downing, T.L., Soto, J., Morez, C., Houssin, T., Fritz, A., Yuan, F., Chu, J., Patel, S., Schaffer, D.V., and Li, S. (2013). Biophysical regulation of epigenetic state and cell reprogramming. Nat. Mater. *12*, 1154–1162.

6. Drummond, D.C., Noble, C.O., Kirpotin, D.B., Guo, Z., Scott, G.K., and Benz, C.C. (2005). Clinical development of histone deacetylase inhibitors as anticancer agents. Annu. Rev. Pharmacol. Toxicol. *45*, 495–528.

7. Gaspar-Maia, A., Alajem, A., Meshorer, E., and Ramalho-Santos, M. (2011). Open chromatin in pluripotency and reprogramming. Nat. Rev. Mol. Cell Biol. *12*, 36–47.

8. Guo, J., Wang, Y., Sachs, F., and Meng, F. (2014). Actin stress in cell reprogramming. Proc Natl Acad Sci USA *111*, E5252-61.

9. Gurdon, J.B. (1962). Adult frogs derived from the nuclei of single somatic cells. Dev. Biol. *4*, 256–273.

10. Gurdon, J.B., and Melton, D.A. (2008). Nuclear reprogramming in cells. Science *322*, 1811–1815.

11. Halley-Stott, R.P., and Gurdon, J.B. (2013). Epigenetic memory in the context of nuclear reprogramming and cancer. Brief. Funct. Genomics *12*, 164–173.

12. Halley-Stott, R.P., Pasque, V., and Gurdon, J.B. (2013). Nuclear

reprogramming. Development *140*, 2468–2471.

13. Ihnatovych, I., Livak, M., Reed, J., de Lanerolle, P., and Strakova, Z. (2009). Manipulating actin dynamics affects human in vitro decidualization. Biol. Reprod. *81*, 222–230.

14. Jain, N., Iyer, K.V., Kumar, A., and Shivashankar, G.V. (2013). Cell geometric constraints induce modular gene-expression patterns via redistribution of HDAC3 regulated by actomyosin contractility. Proc Natl Acad Sci USA *110*, 11349–11354.

15. Karmodiya, K., Krebs, A.R., Oulad-Abdelghani, M., Kimura, H., and Tora, L. (2012). H3K9 and H3K14 acetylation co-occur at many gene regulatory elements, while H3K14ac marks a subset of inactive inducible promoters in mouse embryonic stem cells. BMC Genomics *13*, 424.

16. Kasza, K.E., Nakamura, F., Hu, S., Kollmannsberger, P., Bonakdar, N., Fabry, B., Stossel, T.P., Wang, N., and Weitz, D.A. (2009). Filamin A is essential for active cell stiffening but not passive stiffening under external force. Biophys. J. *96*, 4326–4335.

17. Liao, J.K., Seto, M., and Noma, K. (2007). Rho kinase (ROCK) inhibitors. J. Cardiovasc. Pharmacol. *50*, 17–24.

18. Li, R., Liang, J., Ni, S., Zhou, T., Qing, X., Li, H., He, W., Chen, J., Li, F., Zhuang, Q., et al. (2010). A mesenchymal-to-epithelial transition initiates and is required for the nuclear reprogramming of mouse fibroblasts. Cell Stem Cell *7*, 51–63.

19. Martino, F., Perestrelo, A.R., Vinarský, V., Pagliari, S., and Forte, G. (2018). Cellular mechanotransduction: from tension to function. Front. Physiol. *9*, 824.

20. Roy, B., Venkatachalapathy, S., Ratna, P., Wang, Y., Jokhun, D.S., Nagarajan, M., and Shivashankar, G.V. (2018). Laterally confined growth of cells induces nuclear reprogramming in the absence of exogenous biochemical factors. Proc Natl Acad Sci USA *115*, E4741–E4750.

21. Ruiz, S., Panopoulos, A.D., Herrerías, A., Bissig, K.-D., Lutz, M., Berggren, W.T., Verma, I.M., and Izpisua Belmonte, J.C. (2011). A high proliferation rate is required for cell reprogramming and maintenance of human embryonic stem cell identity. Curr. Biol. *21*, 45–52.

22. Scholzen, T., and Gerdes, J. (2000). The Ki-67 protein: from the known and the unknown. J. Cell. Physiol. *182*, 311–322.

23. Son, M.J., Son, M.-Y., Seol, B., Kim, M.-J., Yoo, C.H., Han, M.-K., and Cho, Y.S. (2013). Nicotinamide overcomes pluripotency deficits and reprogramming barriers. Stem Cells *31*, 1121–1135.

24. Štefková, K., Procházková, J., and Pacherník, J. (2015). Alkaline phosphatase in stem cells. Stem Cells Int. *2015*, 628368.

25. Su, G., Zhao, Y., Wei, J., Han, J., Chen, L., Xiao, Z., Chen, B., and Dai, J. (2013). The effect of forced growth of cells into 3D spheres using low attachment surfaces on the acquisition of stemness properties. Biomaterials *34*, 3215–3222.

26. Takahashi, K., and Yamanaka, S. (2006). Induction of pluripotent stem cells from mouse embryonic and adult fibroblast cultures by defined factors. Cell *126*, 663–676.

27. Takahashi, K., and Yamanaka, S. (2015). A developmental framework for induced pluripotency. Development *142*, 3274–3285.

28. Takahashi, K., and Yamanaka, S. (2016). A decade of transcription factor-mediated reprogramming to pluripotency. Nat. Rev. Mol. Cell Biol. *17*, 183–193.

29. Talwar, S., Kumar, A., Rao, M., Menon, G.I., and Shivashankar, G.V. (2013). Correlated spatio-temporal fluctuations in chromatin compaction states characterize stem cells. Biophys. J. *104*, 553–564.

30. Uhler, C., and Shivashankar, G.V. (2016). Geometric control and modeling of genome reprogramming. Bioarchitecture *6*, 76–84.

31. Vigushin, D.M., Ali, S., Pace, P.E., Mirsaidi, N., Ito, K., Adcock, I., and Coombes, R.C. (2001). Trichostatin A is a histone deacetylase inhibitor with potent antitumor activity against breast cancer in vivo. Clin. Cancer Res. *7*, 971–976.

32. Wang, T., Kang, W., Du, L., and Ge, S. (2017). Rho-kinase inhibitor Y-27632 facilitates the proliferation, migration and pluripotency of human periodontal ligament stem cells. J. Cell. Mol. Med. *21*, 3100–3112.

33. Xu, Y., Wei, X., Wang, M., Zhang, R., Fu, Y., Xing, M., Hua, Q., and Xie, X.

(2013). Proliferation rate of somatic cells affects reprogramming efficiency. J. Biol. Chem. *288*, 9767–9778.